Progress In Electromagnetics Research, PIER 90, 219–233, 2009

A HYBRID METHOD FOR THE ANALYSIS OF RADOME-ENCLOSED HORN ANTENNA

H. F. Meng and W. B. Dou

State Key Laboratory of Millimeter Waves
Southeast University
Nanjing 210096, P. R. China

Abstract—In this paper, the hybrid physical optics/boundary integral-finite element-mode matching (PO/BI-FE-MM) method is proposed for the analysis of the horn antenna enclosed by the electrically large radome. The radome is modeled by the PO method, and the BI-FE-MM method is implemented to the horn region. The equivalent PO currents on the radome surface are coupled into the BI-FE-MM equation of the horn region to account for the effects of the radome on the horn. With this hybrid method, the mutual interactions between the radome and the horn are fully considered. The radiation patterns, field distributions, and the S-parameters of the horns enclosed by different kinds of radome are presented.

1. INTRODUCTION

Dielectric radome is always placed in front of the horn antenna to protect the system from various environments. However, the presence of the radome always affects the radiation properties of the enclosed antenna, such as distorting the radiation pattern, increasing the reflected power at the input port. Therefore, an accurate analysis of the antenna-radome system is very important.

For the electrically large antenna-radome system, the antenna and the radome are always analyzed as they are decoupled. Firstly, the antenna is simulated as the radome is absent, and then the radome is modeled using the decoupled radiation fields from the antenna as the excitation. These analyses ignore the effects of the radome on the antenna [1–10]. In recent years, some researchers have taken the mutual interactions between the antenna and the

Corresponding author: H. F. Meng (menghongfu@163.com).

radome into consideration [11–16]. The radiation patterns and input impedances of the radome-enclosed dipole or slot antennas are analyzed by the integral method [11–14]. The interactions between the reflector antenna and the radome have also been determined by an iterative method [15]. Li et al. have contributed a lot to the analysis of the canonical radome-enclosed circular aperture mounted on an infinite ground plane [17–19].

In this paper, we propose the hybrid PO/BI-FE-MM method for the numerical analysis of the radome-enclosed horn antenna. The present method combines boundary integral (BI), finite element (FE), mode matching (MM), and physical optics (PO). The electrically large radome is modeled by the PO method, and the BI-FE-MM method is implemented to the horn. The reflected fields from the PO currents of the radome surface are coupled back into the BI-FE-MM equation to account for the effects of the radome on the horn. Thus, the mutual couplings between the antenna and the horn are fully considered. The PO/BI-FE-MM method is more accurate than the decoupled antenna-radome analysis, more efficient than the integral method to analyze the electrically large antenna-radome system, and more versatile to analyze various antenna-radome systems. The general formulations and some numerical results of the 2D problems are presented as below.

2. FORMULATIONS

The analysis procedure of the PO/BI-FE-MM method is divided into four steps as shown in Fig. 1. Firstly, the horn is analyzed as the radome is absent, and the equivalent currents J'_a, M'_a on the aperture of the horn are obtained. Then the radome is modeled by the PO method using J'_a, M'_a as the excitation, and the equivalent currents on the radome surface are determined. These two steps are the same as the decoupled antenna-radome analysis [1–10]; however the mutual interactions between the antenna and the radome are ignored. Two additional steps are implemented in the present hybrid analysis. In the third step, the FE method is implemented in the horn region; the MM method is employed at the feeding port to model the excitation, and the BI equation is adopted on the aperture to truncate the FE region in the radiation space. To account for the effects of the radome on the horn, the reflected fields from the PO currents of the radome surface are set as the incident fields to the horn, and are coupled into the BI equation. After solving the hybrid PO/BI-FE-MM equation, the aperture currents of the horn are updated to J_a, M_a. Finally, the radome is analyzed again using the new aperture currents J_a, M_a as the excitation. The radiation fields of the antenna-radome system are

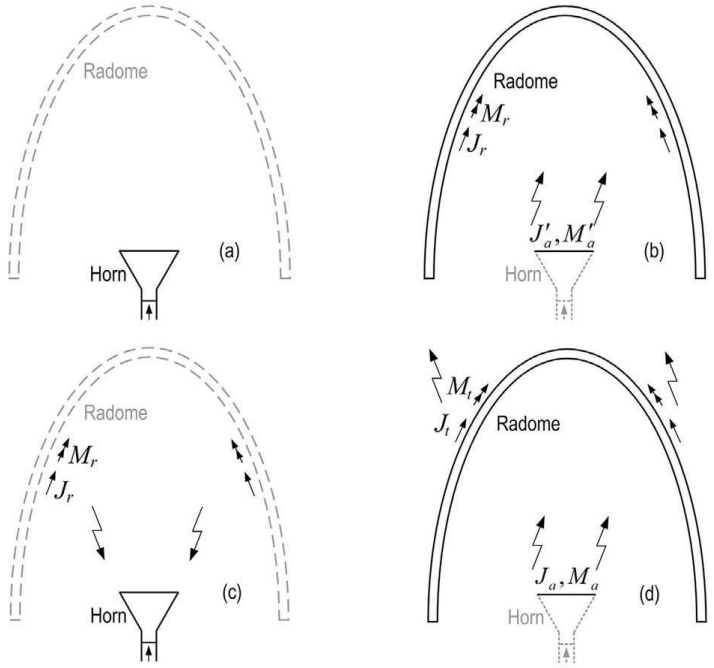

Figure 1. Steps of the PO/BI-FE-MM method: (a) analyzing the horn as the radome is absent; (b) analyzing the radome using the original aperture currents as the excitation; (c) analyzing the horn with the radome effect; (d) analyzing the radome using the new aperture currents as the excitation.

determined by integrating the currents J_t, M_t over the outer surface of the radome. The details of the PO/BI-FE-MM method are shown as below.

2.1. Physical Optics Modeling

The PO method is an efficient high-frequency method for the analysis of the electrically large radome [2, 3, 6]. The general steps are as follows: Firstly, the incident fields on the inner surface of the radome are determined by integrating the aperture currents of the horn. Then, the locally planar assumption is adopted for the smooth radome wall. The incident fields on the inner surface of the radome are decomposed into the perpendicular and parallel polarizations to the plane of incidence. After reflection and transmission by the radome wall, the reflected fields E_r, H_r and the transmitted fields E_t, H_t are

reconstructed on the inner and outer surface of the radome. Finally, the reflected PO currents J_r, M_r on the inner surface and the transmitted PO currents J_t, M_t on the outer surface are obtained by the equivalence principle [3].

$$\begin{aligned} J_r\hat{z} &= \hat{n} \times H_r\hat{\tau} \qquad & M_r\hat{\tau} &= E_r\hat{z} \times \hat{n} \\ J_t\hat{z} &= \hat{n} \times H_t\hat{\tau} \qquad & M_t\hat{\tau} &= E_t\hat{z} \times \hat{n} \end{aligned} \tag{1}$$

where $\hat{n}$, $\hat{\tau}$, and $\hat{z}$ are the unit vectors as in Fig. 2.

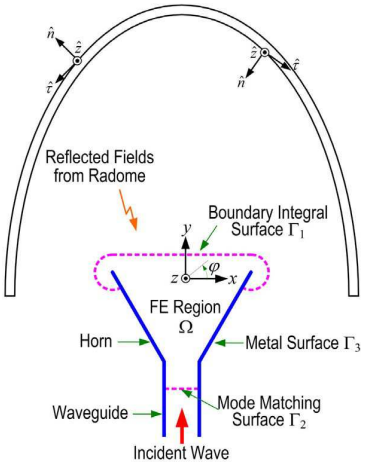

Figure 2. Model of the PO/BI-FE-MM method.

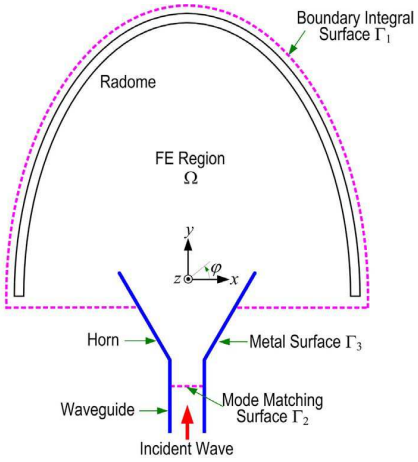

Figure 3. Model of the pure BI-FE-MM method.

2.2. Finite Element Modeling

The electrical field E_z in the FE region shown in Fig. 2 satisfies the following Helmholtz equation [20]

$$\begin{cases} \dfrac{\partial}{\partial x}\left(\dfrac{1}{\mu_r}\dfrac{\partial E_z}{\partial x}\right)+\dfrac{\partial}{\partial y}\left(\dfrac{1}{\mu_r}\dfrac{\partial E_z}{\partial y}\right)+k_0^2\varepsilon_r E_z = 0 & \text{in } \Omega \\ \dfrac{1}{\mu_r}\dfrac{\partial E_z}{\partial n} = jk_0 Z_0 J_a & \text{on } \Gamma_1 \\ E_z = E_{WG} & \text{on } \Gamma_2 \\ E_z = 0 & \text{on } \Gamma_3 \end{cases} \tag{2}$$

where Ω is the inner area of the FE region, Γ_1, Γ_2, and Γ_3 are the boundaries shown in Fig. 2, J_a is the unknown electrical current on

the aperture, and E_{WG} is the field in the waveguide, which will be discussed later.

The variational approach to determine the field E_z is to consider the functional

$$F(E_z) = \frac{1}{2}\iint_{\Omega}\left[\frac{1}{\mu_r}\left(\frac{\partial E_z}{\partial x}\right)^2 + \frac{1}{\mu_r}\left(\frac{\partial E_z}{\partial y}\right)^2 - k_0^2\varepsilon_r E_z^2\right]dS + jk_0 Z_0\int_{\Gamma 1} E_z J_a d\Gamma \tag{3}$$

which is stationary for the solution of (2) [20].

Then, the FE region Ω is meshed with small triangles. The field E_z is expanded in terms of the finite element function ϕ_i defined in the triangular meshes, and J_a is expanded using the triangular basis function. Substituting the expansion functions into $F(E_z)$ and enforcing the first-order variation of the functional to be $\delta F(E_z) = 0$, a linear equation can be obtained [20]

$$\begin{bmatrix} K_{II} & K_{IS} & 0 & C \\ K_{SI} & K_{SS} & B & 0 \end{bmatrix}\begin{bmatrix} E_z \\ M_a \\ J_a \\ e^r \end{bmatrix} = \begin{bmatrix} 0 \\ 0 \end{bmatrix} \tag{4}$$

where E_z is the electrical field in Ω, e^r will be discussed in Subsection 2.4. M_a is the equivalent magnetic current on Γ_1, which has the relationship with the aperture field as

$$M_a\hat{\tau} = E_z\hat{z}\times\hat{n}. \tag{5}$$

2.3. Boundary Integral Equation

The electrical field E_z on Γ_1 satisfies the following BI equation

$$E_z - E(J_a, M_a) = E(J_r, M_r) \tag{6}$$

where $E(J_a, M_a)$ is the radiation field of the aperture currents, $E(J_r, M_r)$ is the field radiated from the reflected PO currents determined in Subsection 2.1, and the operator $E(J, M)$ is defined as

$$E(J, M) = -jk_0 Z_0\int_{\Gamma} J(r')\, G(r, r')\, dr' + \int_{\Gamma} M(r')\,\frac{\partial G(r, r')}{\partial n'}dr' \tag{7}$$

in which $G(r, r')$ is the Green's function in free space, and r', r are the source and field points respectively.

This BI equation couples the reflected fields of the radome into the boundary condition of the horn analysis. As we have the relationship of (5), expanding the currents J_a, M_a with the triangular basis function and employing the Galekin's type method of moments, the linear matrix of the BI equation is obtained, and is given by

$$[P \quad Q] \begin{bmatrix} M_a \\ J_a \end{bmatrix} = [b]. \tag{8}$$

2.4. Mode Matching Method [21]

In the FE region, the field has been interpolated by the finite element function ϕ_i, and then the field E_z at the feeding port Γ_2 is

$$E_z = \sum_{i=1}^{N} A_i \phi^i (x, y) \tag{9}$$

which only has the relationship with the nodes on Γ_2.

In the waveguide, it is assumed that the incident field only has the dominant mode

$$E^{in} = e_{01}^{in} \sin (x + a/2) \frac{\pi}{a} \exp (-j\beta y) \tag{10}$$

where a is the width of the waveguide, β is the propagation constant of the dominant mode, and e_{01}^{in} is the amplitude of the incident wave.

Besides the dominant modes, many higher modes may be reflected back to the waveguide. So, the reflected field on the boundary Γ_2 is the sum of all the modes

$$E^{ref} = \sum_{n=1}^{L} e_{0n}^{r} \sin (x + a/2) \frac{n\pi}{a} \exp (j\beta_n y). \tag{11}$$

Thus, the total field at the feeding port Γ_2 of the waveguide is

$$E_{WG} = E^{in} + E^{ref}. \tag{12}$$

As the fields on both sides of Γ_2 must be continuous, we has the third formula in (2), and it is expressed as

$$\begin{aligned} \sum_{i=1}^{N} A_i \phi^i \;=\; & e_{01}^{in} \sin (x + a/2) \frac{\pi}{a} \exp (-j\beta y) \\ & + \sum_{n=1}^{L} e_{0n}^{r} \sin (x + a/2) \frac{n\pi}{a} \exp (j\beta_n y). \end{aligned} \tag{13}$$

By multiplying $\sin(x + a/2)(m\pi/a)$ on both sides of (13), and integrating from $[-a/2, a/2]$ for x on Γ_2, we obtain the following linear equation

$$[D \quad T] \begin{bmatrix} E_z \\ e^r \end{bmatrix} = [s] \tag{14}$$

where $e^r = [e^r_{01}, e^r_{02}, \ldots, e^r_{0L}]^T$ are the coefficients of the reflected modes, D, T, and s are the coefficient matrices as in [21].

2.5. Hybridization

By adding E_z and e^r in the unknown column of (8) and adding zeros in the matrix, we get a same-result equation of (8) as follows:

$$[0 \quad P \quad Q \quad 0] \begin{bmatrix} E_z \\ M_a \\ J_a \\ e^r \end{bmatrix} = [b] \tag{15}$$

We can do the same transformation to (14), and we obtain

$$[D \quad 0 \quad 0 \quad T] \begin{bmatrix} E_z \\ M_a \\ J_a \\ e^r \end{bmatrix} = [s] \tag{16}$$

As we can see, (4), (15), and (16) have the same unknowns. Combining them, we get the hybrid equation of the PO/BI-FE-MM method:

$$\begin{bmatrix} K_{II} & K_{IS} & 0 & C \\ K_{SI} & K_{SS} & B & 0 \\ 0 & P & Q & 0 \\ D & 0 & 0 & T \end{bmatrix} \begin{bmatrix} E_z \\ M_a \\ J_a \\ e^r \end{bmatrix} = \begin{bmatrix} 0 \\ 0 \\ b \\ s \end{bmatrix} \tag{17}$$

Solving this equation, the currents J_a, M_a on the aperture of the horn and the coefficients of all the reflected modes at the feeding port are obtained. These aperture currents are used for the radome analysis again as the new excitation as in Subsection 2.1. The radiation fields of the antenna-radome system are determined by integrating the equivalent currents J_t, M_t over the outer surface of the radome.

The S-parameter at the feeding port of the waveguide is given by

$$S_{11} = 20 \log \left(e^r_{01} / e^{in}_{01} \right) \tag{18}$$

3. NUMERICAL RESULTS

3.1. Verification of the PO/BI-FE-MM Method

As the first validation example, a horn antenna enclosed by a hemispherical radome is analyzed. The radome is single layer with the inner radius of 31.90 mm and the thickness of 3.19 mm. The radome wall is lossless dielectric with the relative permittivity of $\varepsilon_r = 2.0$. The aperture of the horn is 20.00 mm. It is fed by a waveguide with the width of 2.54 mm. The incident electrical field at the center of the waveguide is set to be 1.0 V/m, and the operating frequency is 94 GHz.

In order to verify the validity of the PO/BI-FE-MM method, a full wave method as shown in Fig. 3 is also proposed. The dielectric radome is included into the FE region and no approximation is adopted between the antenna and the radome, so it is called the pure BI-FE-MM method. As this is a full wave method, the result is regarded as the exactly referenced solution.

The radiation patterns of the antenna-radome system determined by the PO/BI-FE-MM method and the decoupled antenna-radome analysis [2] are compared in Fig. 4. The pattern obtained by the full wave method is also given as a reference. Obviously, there are significant differences between the decoupled radiation pattern and the one determined by the present method. The pattern determined by the PO/BI-FE-MM method has good agreement with the one of the full wave method from 45° to 135°. Although there are still some differences between the two patterns in the far angle region, which are due to the neglect of the interactions among the radome itself in the present method; however, we do not care about them as they are lower than −25 dB.

The field distributions in the radome-enclosed horn determined by the PO/BI-FE-MM method and the full wave method are compared

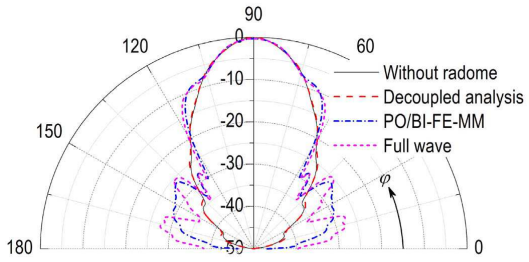

Figure 4. Radiation patterns of the radome-enclosed horn determined by different methods.

with the field distribution of the horn without radome in Fig. 5. Clearly, the field distribution in the horn is significantly affected by the radome, and the present method predicts the influences of the radome on the horn exactly. The S_{11} at the feeding port of the waveguide determined by these two methods are -22.12 dB and -22.43 dB respectively, which are also in good agreement.

The present PO/BI-FE-MM method only takes 10 minutes to analyze this antenna-radome system; however, the full wave method spends about 2 hours 4 minutes. The efficiency of the proposed method is very high and the accuracy of the result is acceptable.

3.2. Hemispherical Radome-enclosed Horn

Then, we analyze the same horn antenna enclosed by a lossy hemispherical radome with the same inner radius as the first example. This radome wall is 1.60 mm in thickness and with the dielectric of $\varepsilon_r = 4.0$ and $\tan\delta = 0.002$. The field distributions in the radome-enclosed horn at 94 GHz, 96 GHz, and 100 GHz are depicted in Fig. 6. As we can see, when the radome is covered, the field distribution in the horn at 94 GHz is nearly the same as that without radome in Fig. 5(a); however, some standing waves appear in the horn at 96 GHz, and are more significant at 100 GHz. The radiation patterns of the horn without radome or with the hemispherical radome at the three frequencies are compared in Figs. 7(a) and (b). It can be seen that the radiation property of the horn without radome has little changes with the frequency; however, when the radome is covered, the radiation patterns of the antenna-radome system are changed significantly.

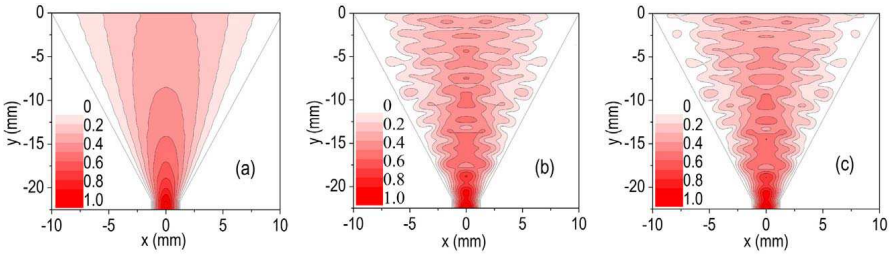

Figure 5. Electrical field distributions in the horn: (a) without radome; (b) with radome determined by the PO/BI-FE-MM method; (c) with radome determined by the full wave method.

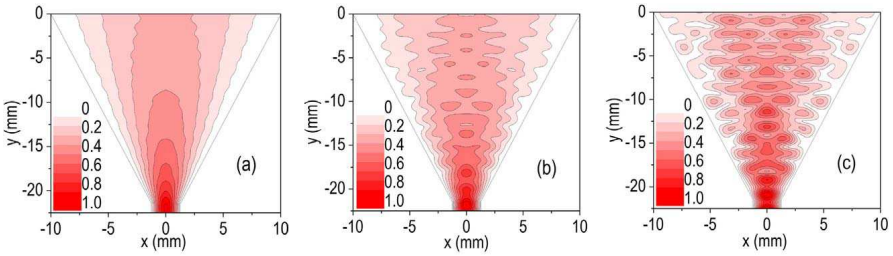

Figure 6. Electrical field distributions in the horn enclosed by the hemispherical radome: (a) 94 GHz; (b) 96 GHz; (c) 100 GHz.

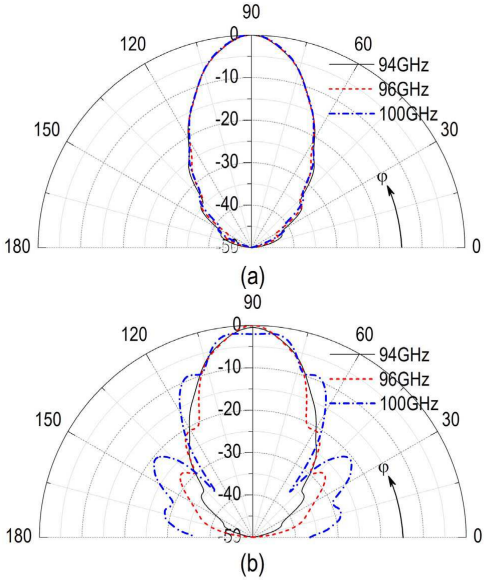

Figure 7. Radiation patterns of the horn without or with the radome at 94 GHz, 96 GHz, and 100 GHz: (a) without radome; (b) with the hemispherical radome.

3.3. Elliptical Radome-enclosed Horn

Another example is the same horn antenna enclosed by an elliptical radome. The radome is 65.40 mm in height and 67.00 mm in base diameter. The thickness and dielectric of the elliptical radome are the same as those of the hemispherical one. Fig. 8 shows the field distributions in the elliptical radome-enclosed horn at 94 GHz, 96 GHz, and 100 GHz, and Fig. 9 depicts the radiation patterns of the antenna-

radome system. It is demonstrated that the radome also has different interactions on the horn at different frequencies. Compared with the field distributions in the hemispherical radome-enclosed horn in Fig. 6, the influence of the elliptical radome on the horn is bigger than the hemispherical one at 94 GHz; however, it is much smaller at 96 GHz and 100 GHz.

For the horn without radome, the S_{11} at the feeding port is lower than -30 dB from 90 GHz to 100 GHz as shown in Fig. 10. However, as observed in Fig. 6 and Fig. 8, the radomes induce obvious standing waves in the horn, which certainly affect the S-parameters at the feeding port. When the hemispherical radome is covered, the S_{11} has little change at 94 GHz, and is significantly raised in other frequencies. However, the S_{11} of the elliptical radome-enclosed horn is higher in the low frequency band and lower in the high frequency band than the hemispherical one.

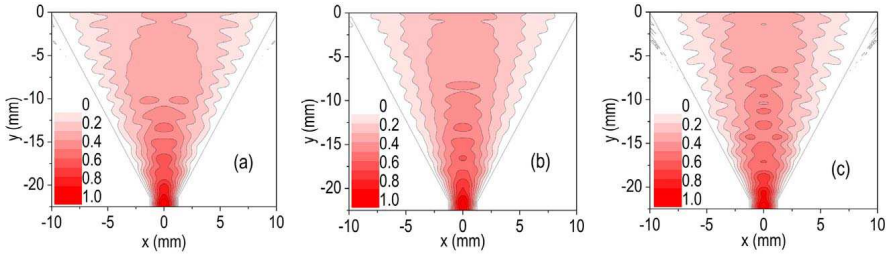

Figure 8. Electrical field distributions in the horn enclosed by the elliptical radome: (a) 94 GHz; (b) 96 GHz; (c) 100 GHz.

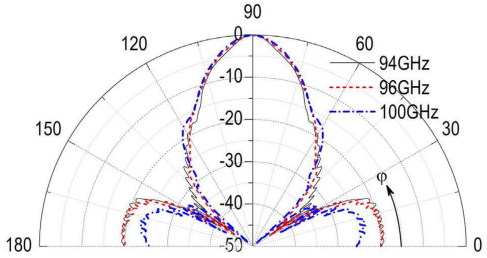

Figure 9. Radiation patterns of the horn enclosed by the elliptical radome at 94 GHz, 96 GHz, and 100 GHz.

3.4. A-sandwich Von-Karman Radome-enclosed Horn

The last example is an A-sandwich Von-Karman radome. This radome has two high-density dielectric skins separated by a low-density core having a lower relative permittivity than the skins. The parameters of the antenna and the radome are given in Fig. 11(a). This antenna-radome works at 10 GHz. The radiation patterns of the horn without or with the radome are illustrated in Fig. 11(b). It is clear that the radome induces an attenuation of 1.1 dB in the main lobe, and some side lobes appear in the far angle region. The S_{11} at the feeding port is also increased from -34 dB to -22 dB.

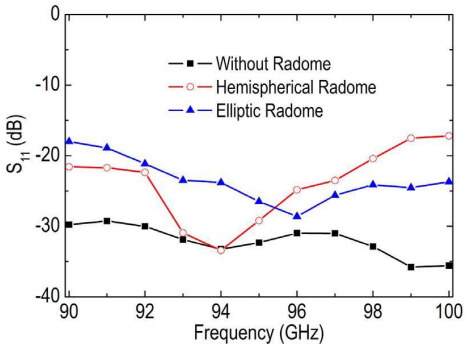

Figure 10. S_{11} of the horn enclosed by the hemispherical radome or the elliptical radome.

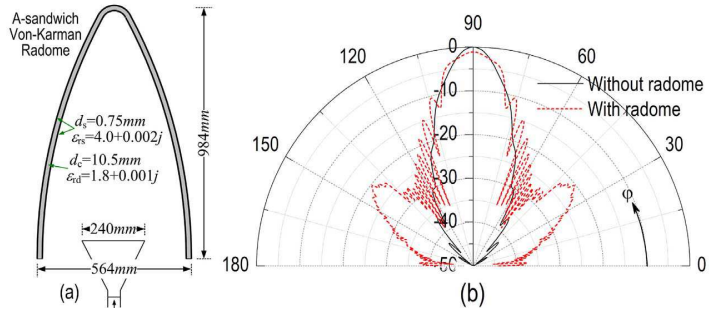

Figure 11. Configuration and radiation pattern of the horn enclosed by the A-sandwich Von-Karman radome: (a) configuration, (b) radiation patterns.

4. CONCLUSION

In this paper, we have proposed a hybrid concept for the numerical analysis of the electrically large radome-enclosed horn antenna. This hybrid method combines BI, FE, MM, and PO to couple the interactions between the radome and the horn into the antenna-radome analysis. The validation example verifies that the PO/BI-FE-MM method is more accurate than the traditional decoupled antenna-radome analysis, and more efficient to save the computational time than the full wave method. Also, the versatility of this method for the analysis of the horn enclosed by various radomes is confirmed by several numerical examples. The results show that the radiation properties of the horn are affected by different radomes at different frequencies.

ACKNOWLEDGMENT

This work is supported by the National Natural Science Foundation of China under grant 60571028.

REFERENCES

1. Tricoles, G., "Radiation patterns of a microwave antenna enclosed by a hollow dielectric wedge," *Journal of Optical Society of America*, Vol. 53, No. 5, 545–557, 1963.
2. Paris, D., "Computer-aided radome analysis," *IEEE Trans. Antennas Propagat.*, Vol. 18, No. 1, 7–15, 1970.
3. Wu, D. C. F. and R. C. Rudduck, "Plane wave spectrum-surface integration technique for radome analysis," *IEEE Trans. Antennas Propagat.*, Vol. 22, No. 5, 497–500, 1974.
4. Arvas, E., A. Rahhalarabi, U. Pekel, and E. Gundogan, "Electromagnetic transmission through a small radome of arbitrary shape," *Microwaves, Antennas and Propagation, IEE Proceedings H*, Vol. 137, No. 6, 401–405, 1990.
5. Gordon, R. K. and R. Mittra, "Finite element analysis of axisymmetric radomes," *IEEE Trans. Antennas Propagat.*, Vol. 41, No. 7, 975–981, 1993.
6. Abdel Moneum, M. A., Z. X. Shen, J. L. Volakis, and O. Graham, "Hybrid PO-MoM analysis of large axi-symmetric radomes," *IEEE Trans. Antennas Propagat.*, Vol. 49, No. 12, 1657–1666, 2001.
7. Lu, C. C., "A fast algorithm based on volume integral equation

for analysis of arbitrarily shaped dielectric radomes," *IEEE Trans. Antennas Propagat.*, Vol. 51, No. 3, 606–612, 2003.

8. Nie, X.-C., N. Yuan, L.-W. Li, T.-S. Yeo, and Y.-B. Gan, "Fast analysis of electromagnetic transmission through arbitrary shaped airborne radomes using precorrected-FFT method," *Progress In Electromagnetics Research*, PIER 54, 37–59, 2005.
9. Kedar, A. and U. K. Revankar, "Parametric study of flat sandwich multilayer radome," *Progress In Electromagnetics Research*, PIER 66, 253–265, 2006.
10. Zou, Y. L., J. Y. Li, and Q. Z. Liu, "Modified mode decomposition for analyzing antennas with body of revolution radome," *Journal of Electromagnetic Waves Applications*, Vol. 21, No. 10, 1403–1410, 2007.
11. Nie, X. C., Y. B. Gan, N. Yuan, and C. F. Wang, "An efficient hybrid method for analysis of slot arrays enclosed by a large radome," *Journal of Electromagnetic Waves Applications*, Vol. 20, No. 2, 249–264, 2006.
12. Zhao, W. J., Y. B. Gan, L. W. Li, and C. F. Wang, "Effects of an electrically large airborne radome on radiation patterns and input impedance of a dipole array," *IEEE Trans. Antennas Propagat.*, Vol. 55, No. 8, 2399–2402, 2007.
13. He, M., X. W. Xu, B. Hu, and Y. Zheng, "Accurate analysis of arbitrarily shaped wire antenna-dielectric radome structures," *IEEE Antennas and Wireless Propagation Letters*, Vol. 6, 408–410, 2007.
14. He, M., "On the characteristics of radome enclosed Archimedean spiral antennas," *IEEE Trans. Antennas Propagat.*, Vol. 56, No. 7, 1867–1874, 2008.
15. Oguzer, T. and A. Altintas, "Analysis of the nonconcentric reflector antenna-in-radome system by the iterative reflector antenna and radome interaction," *Journal of Electromagnetic Waves Applications*, Vol. 21, No. 1, 57–70, 2007.
16. Hémon, R., P. Pouliguen, H. He, J. Saillard, and J.-F. Damiens, "Computation of EM field scattered by an open-ended cavity and by a cavity under radome using the iterative physical optics," *Progress In Electromagnetics Research*, PIER 80, 77–105, 2008.
17. Leong, M. S., L. W. Li, X. Ma, et al., "Analysis of total transmission loss and cross-polarization of a hemi-spherical dielectric radome with rain-water layer: A closed form solution," *Journal of Electromagnetic Waves Applications*, Vol. 12, No. 6, 731–752, 1998.

18. Li, L.-W., L. Zhou, M. S. Leong, T.-S. Yeo, and P. S. Kooi, "An open-ended circular waveguide with an infinite conducting flange covered by a dielectric hemi-spherical radome shell: Full wave analysis and Green dyadics," *Progress In Electromagnetics Research*, PIER 21, 221–245, 1999.
19. Li, L. W., M. S. Leong, and J. A. Kong, "An alternative representation of magnetic Green's dyadics in a spherical-shell dielectric radome," *Journal of Electromagnetic Waves Applications*, Vol. 16, No. 1, 63–77, 2002.
20. Jin, J. M., *The Finite Element Method in Electromagnetics*, Wiley, New York, 1993.
21. Wu, H. C. and W. B. Dou, "A rigorous analysis and experimental researches of waveguide magic tee at W band," *Progress In Electromagnetics Research*, PIER 60, 131–142, 2006.